

**LARGE-EDDY SIMULATION OF NASA LaRC
COAXIAL He-O₂/AIR JET**

by

Mahdi Mohebbi

Submitted to the Graduate Faculty of
the School of Engineering in partial fulfillment
of the requirements for the degree of

Master of Science

University of Pittsburgh

2007

UNIVERSITY OF PITTSBURGH
SCHOOL OF ENGINEERING

This thesis was presented

by

Mahdi Mohebbi

It was defended on

July 23, 2007

and approved by

P. Givi, Ph.D., William K. Whiteford Professor

S. K. Cho, Ph.D., Assistant Professor

L. Schaefer, Ph.D., Associate Professor

Thesis Advisor: P. Givi, Ph.D., William K. Whiteford Professor

LARGE-EDDY SIMULATION OF NASA LaRC COAXIAL He-O₂/AIR JET

Mahdi Mohebbi, M.S.

University of Pittsburgh, 2007

Large-eddy simulation (LES) is conducted of a coaxial jet flow configuration. This configuration was previously considered in the laboratory experiments at the Hypersonic Air-breathing Propulsion Branch at the NASA Langley Research Center (LaRC). It consists of a coaxial jet discharging into stagnant air with a main stream of He-O₂ (95% helium and 5% oxygen by volume) and a coflow of air. The objective of this work is to investigate the performance of conventional LES models for supersonic flows. In the simulations, the filtered, compressible, 3-dimensional Navier-Stokes equations for a multi-species system are solved. The subgrid scale closure is attained using the generalized Smagorinsky^{13,14,25,41} model and the dynamic model.²⁹ The predicted results are assessed via comparison with data from the NASA LaRC.

TABLE OF CONTENTS

1.0 INTRODUCTION	1
2.0 FORMULATION	3
2.1 Governing Equations	3
2.2 Subgrid Scale (SGS) Closure	7
3.0 CONFIGURATION AND COMPUTATION	10
4.0 RESULTS	13
5.0 CONCLUSIONS	23
BIBLIOGRAPHY	24

LIST OF TABLES

1	Model constants.	9
2	Summary of flow and calculations parameters.	12

LIST OF FIGURES

1	Schematics of the coaxial jet facility	11
2	Average filtered velocity profiles	14
3	Profiles of average filtered mass fraction of center jet	15
4	Computed values of Smagorinsky coefficient from dynamic Simulations	16
5	Computed SGS Prandtl and Schmidt numbers from dynamic Simulations	16
6	Resolved and residual portions of turbulent stresses and fluxes	17
7	Contour plot of the instantaneous values of $\langle p \rangle_t$ (kPa) at $t^+ = 71.67$ (Simulation III).	19
8	Contour plot of the Reynolds averaged values of the Mach number (Simulation III).	20
9	Contour plot of the instantaneous values of the filtered density (kg/m^3) at $t^+ = 299.13$ (Simulation I).	21
10	Contour plot of the Reynolds averaged values of $\langle Y_{He-O_2} \rangle_L$ from Simulation I.	22

NOMENCLATURE

C_I	Yoshizawa coefficient.
C_p	Mass specific heat of mixture at constant pressure.
C_s	Smagorinsky coefficient.
\mathcal{D}_α	Diffusion coefficient of species α .
E	Total energy.
\mathcal{G}	LES filter function.
L_{ref}	Reference length.
Le_α	Lewis number ($= \lambda/(\rho C_p \mathcal{D}_\alpha)$).
M_i^α	Mass flux vector of species α (2.3).
Ma	Mach number.
\mathcal{M}_i^α	SGS mass flux vector of species α (2.10).
N_x, N_y and N_z	Number of grid points in x -, y - and z -directions, respectively.
Pr_T	SGS Prandtle number.
Q_i	Energy flux vector (2.5).
\mathcal{Q}_i	SGS energy flux vector (2.12).
$\mathcal{Q}_i^{(c)}$	SGS chemical energy flux vector (2.29).
$\mathcal{Q}_i^{(k)}$	SGS turbulent diffusion vector (2.30).
$\mathcal{Q}_i^{(s)}$	SGS heat flux vector (2.28).
R	Specific gas constant of the mixture.
$R(f_i, f_j)$	Resolved portion of the correlation between f_i and f_j (4.1).
Re_D	Reynolds number based on inlet jet properties.
S_{ij}	Rate of strain tensor.
Sc_T	SGS Schmidt number.

\mathcal{S}_{ij}	SGS stress tensor (2.11).
$\mathcal{S}_{ij}^{(D)}$	Deviatoric part of the SGS stress tensor (2.21).
$\mathcal{S}_{ij}^{(I)}$	Isotropic part of the SGS stress tensor (2.22).
T	Absolute temperature.
U_{ref}	Reference velocity.
x, y, z	Spatial Coordinates.
Y_α	Mass fraction of species α .
e	Sensible energy of mixture ($= RT/(\gamma - 1)$).
h_f^0	Mass enthalpy of formation of mixture at 0 K.
$h_{f,\alpha}^0$	Mass enthalpy of formation of species α at 0 K.
l	Characteristic filter length ($= (\Delta_x \Delta_y \Delta_z)^{\frac{1}{3}}$).
p	Thermodynamic pressure.
t	Time.
t^+	Non-dimensional time.
u_i	Components of velocity vector.
\vec{x}	Position vector.
Ω	The entire flow domain.
Δ_x, Δ_y and Δ_z	Grid Spacing in x -, y - and z -directions, respectively.
γ	Ratio of specific heats of mixture at constant pressure and constant volume.
λ	Heat conductivity of mixture.
μ	Dynamic viscosity of mixture.
ν_T	SGS viscosity (2.25).
ρ	Mass density.
σ_{ij}	Stress tensor (2.4).
$\tau^R(f_i, f_j)$	Residual portion of the correlation between f_i and f_j (4.2).
\bar{f}	Average value of f .
$\langle f \rangle_t$	Filtered value of variable f .

$\langle f \rangle_L$

Favre filtered of variable f .

ACKNOWLEDGMENT

The knowledge I have gained in turbulence and specifically in large-eddy simulation is primarily from my advisor, Prof. Peyman Givi, to whom goes my extreme gratitude for all his support and patience. I am also indebted to Drs. M. Reza H. Sheikhi and Tomasz G. Drozda for their help to bring me up to speed. Dr. Sheikhi also helped me with the problem formulation and solution. Thanks also go to my colleagues at the Computational Transport Phenomena Laboratory at the University of Pittsburgh, Mr. S. Levent Yilmaz, Mr. S. Mehdi B. Nik and Mr. Patrick Pisciuneri for all the sincere help. This work was supported by the Office of the Secretary of Defense (OSD) under AFSOR contract FA9101-04-C-0014. Computational resources for simulations were partly provided by the National Center for Supercomputing Applications (NCSA) and the Pittsburgh Supercomputing Center (PSC).

1.0 INTRODUCTION

It is now widely accepted that the optimum means of capturing the detailed, unsteady physics of turbulent combustion is via large-eddy simulation (LES).^{20,30} A serious issue associated with LES is accurate modeling of the subgrid scale (SGS) quantities.^{1,30} The filtered density function (FDF) methodology^{20,32} has proven particularly effective for this closure. The FDF is the counterpart of the probability density function (PDF) methodology in Reynolds-averaged simulation, commonly referred to as Reynolds-averaged Navier-Stokes (RANS) of turbulent reacting flows.^{27,32}

The idea of using the PDF method for LES was first suggested by Givi.¹⁹ But it was the formal definition of FDF by Pope³¹ which provided the mathematical foundation of LES/FDF. Within the past several years, steady progress has been made in developments and applications of the FDF methodology. In its simplest form, the “assumed” FDF method was suggested by Madnia *et al.*,^{15,28} where all of the drawbacks of this simple approach were highlighted.

Similar to PDF methods, there are different ways by which the FDF can be considered. These differ in the flow variables which are being considered (*e.g.* the scalar variables describing the thermochemistry, or additionally the components of the velocity), and whether the method is applicable to constant density or variable density flows. The marginal scalar FDF (SFDF) was developed by Colucci *et al.*² This work demonstrated, for the first time, that solution of the transported FDF is possible. The encouraging results obtained in this work motivated further research on this methodology. The scalar filtered mass density function (SFMDf), which is the variable density form of SFDF was developed by Jaber *et al.*²⁴ and Garrick *et al.*¹⁶ The marginal velocity FDF (VFDF) was developed by Gicquel *et al.*^{17,18} The joint velocity-scalar FDF (VSFDF) was developed by Sheikhi *et al.*³⁶ The work on joint

velocity-scalar FMDF (VSFMDF), which is the variable form of VSFDF has just been completed.^{8,35} The first LES of a realistic flame (Sandia's piloted diffusion flame D) was recently conducted via SFMDF.³⁷ Prediction of the more complex field of a bluff-body (Sydney Flame) by LES/FDF has just been finished.^{7,8}

Work is underway at the University of Pittsburgh to develop the FDF method for LES of high speed turbulent reacting flows. This work is part of a joint collaboration with the NASA LaRC.¹² The ultimate goal is to develop a high fidelity LES/FDF method with inclusion of realistic chemical kinetics models. This thesis, is focused on investigation of conventional hydrodynamic LES models in high speed flows. These flows are of significant interest to NASA and have long been the subject of computational and experimental research in the Hypersonic Airbreathing Propulsion activities there.^{3,5,9-11,39} The models appraised in this Thesis are appropriate to use in LES via SFMDF.

2.0 FORMULATION

2.1 GOVERNING EQUATIONS

The governing equations for a compressible turbulent flow involving N , non-reacting species are³⁰:

$$(2.1a) \quad \frac{\partial \rho}{\partial t} + \frac{\partial(\rho u_i)}{\partial x_i} = 0,$$

$$(2.1b) \quad \frac{\partial(\rho Y_\alpha)}{\partial t} + \frac{\partial(\rho u_i Y_\alpha)}{\partial x_i} = \frac{\partial M_i^\alpha}{\partial x_i},$$

$$(2.1c) \quad \frac{\partial(\rho u_i)}{\partial t} + \frac{\partial(\rho u_i u_j)}{\partial x_j} = -\frac{\partial p}{\partial x_i} + \frac{\partial \sigma_{ij}}{\partial x_j},$$

$$(2.1d) \quad \frac{\partial(\rho E)}{\partial t} + \frac{\partial(\rho E u_i)}{\partial x_i} = -\frac{\partial(p u_i)}{\partial x_i} + \frac{\partial Q_i}{\partial x_i} + \Phi,$$

where $\rho(\vec{\mathbf{x}}, t)$ is the mass density of the fluid, $u_i(\vec{\mathbf{x}}, t)$ ($i = 1, 2, 3$), is the i -th component of velocity, $Y_\alpha(\vec{\mathbf{x}}, t)$ ($\alpha = 1, 2, \dots, N$) is the mass fraction of species α , $p(\vec{\mathbf{x}}, t)$ is the thermodynamic pressure and $E(\vec{\mathbf{x}}, t)$ is the total energy of the fluid. In the above, $\vec{\mathbf{x}}$ is the position vector and t is the time coordinate. The mass flux, M_i^α , the stress tensor, σ_{ij} , the energy flux⁴⁰, Q_i , and the viscous dissipation Φ , are given by

$$(2.2) \quad \Phi = \frac{\partial(\sigma_{ij} u_i)}{\partial x_j},$$

$$(2.3) \quad M_i^\alpha = \rho \mathcal{D}_\alpha \frac{\partial Y_\alpha}{\partial x_i},$$

$$(2.4) \quad \sigma_{ij} = \mu \left(\frac{\partial u_i}{\partial x_j} + \frac{\partial u_j}{\partial x_i} - \frac{2}{3} \frac{\partial u_k}{\partial x_k} \delta_{ij} \right),$$

$$(2.5) \quad Q_i = \frac{\lambda}{C_p} \left(\frac{\partial E}{\partial x_i} + \frac{\partial(p/\rho)}{\partial x_i} - \frac{1}{2} \frac{\partial(u_j u_j)}{\partial x_i} \right),$$

where \mathcal{D}_α is the diffusion coefficient of species α in the rest of the mixture and μ , λ and C_p are the mixture dynamic viscosity, heat conductivity and mass specific heat at constant pressure, respectively. Equation (2.3) implies the Fick's law. In the energy flux, the Dufour effect is ignored and the Lewis number, $Le_\alpha = \lambda/(\rho C_p \mathcal{D}_\alpha)$, is assumed to be unity for all species. These equations are supplemented by the equation of state:

$$(2.6) \quad p = \rho R T,$$

where R is the specific gas constant of the mixture and $T(\vec{\mathbf{x}}, t)$ denotes the temperature. The relation between the total energy, E , and the sensible energy, e , is:⁹

$$(2.7) \quad e = E - h_f^o - \frac{u_i u_i}{2},$$

where h_f^o is the mass enthalpy of formation of the mixture at 0 K and $e = RT/(\gamma - 1)$, with γ being the ratio of mixture's specific heats at constant pressure and constant volume. It is assumed that the mixture properties do not change with temperature.

In LES, the above equations are filtered:²⁶

$$(2.8) \quad \langle f(\vec{\mathbf{x}}, t) \rangle_l = \int_{\Omega} f(\vec{\mathbf{x}}', t) \mathcal{G}(\vec{\mathbf{x}} - \vec{\mathbf{x}}', t; l) d\vec{\mathbf{x}}',$$

where \mathcal{G} is a spatially homogeneous, temporally invariant filter function with the property:

$$\int_{\Omega} \mathcal{G}(\vec{\mathbf{x}} - \vec{\mathbf{x}}', t; l) d\vec{\mathbf{x}}' = 1.$$

Here l denotes the characteristic filter length and the integration is carried out over the entire domain, Ω . In compressible flows, it is more convenient to use the density-weighted (Favre) filtering:²²

$$\langle f \rangle_L = \frac{\langle \rho f \rangle_l}{\langle \rho \rangle_l}.$$

Application of the filtering operation to (2.1) yields:

$$(2.9a) \quad \frac{\partial \langle \rho \rangle_l}{\partial t} + \frac{\partial (\langle \rho \rangle_l \langle u_i \rangle_L)}{\partial x_i} = 0,$$

$$(2.9b) \quad \frac{\partial (\langle \rho \rangle_l \langle Y_\alpha \rangle_L)}{\partial t} + \frac{\partial (\langle \rho \rangle_l \langle u_i \rangle_L \langle Y_\alpha \rangle_L)}{\partial x_i} = \frac{\partial \langle M_i^\alpha \rangle_l}{\partial x_i} + \frac{\partial \mathcal{M}_i^\alpha}{\partial x_i},$$

$$(2.9c) \quad \frac{\partial (\langle \rho \rangle_l \langle u_i \rangle_L)}{\partial t} + \frac{\partial (\langle \rho \rangle_l \langle u_i \rangle_L \langle u_j \rangle_L)}{\partial x_j} = -\frac{\partial \langle p \rangle_l}{\partial x_i} + \frac{\partial \langle \sigma_{ij} \rangle_l}{\partial x_j} + \frac{\partial \mathcal{S}_{ij}}{\partial x_j},$$

$$(2.9d) \quad \frac{\partial (\langle \rho \rangle_l \langle E \rangle_L)}{\partial t} + \frac{\partial (\langle \rho \rangle_l \langle E \rangle_L \langle u_i \rangle_L)}{\partial x_i} = -\frac{\partial \langle p u_i \rangle_l}{\partial x_i} + \frac{\partial \langle Q_i \rangle_l}{\partial x_i} + \langle \Phi \rangle_l + \frac{\partial \mathcal{Q}_i}{\partial x_i},$$

where the subgrid scale (SGS) mass flux, \mathcal{M}_i^α , the SGS stress tensor, \mathcal{S}_{ij} , and the SGS heat flux, \mathcal{Q}_i , are defined as:

$$(2.10) \quad \mathcal{M}_i^\alpha = -\langle \rho \rangle_l [\langle u_i Y_\alpha \rangle_L - \langle u_i \rangle_L \langle Y_\alpha \rangle_L],$$

$$(2.11) \quad \mathcal{S}_{ij} = -\langle \rho \rangle_l [\langle u_i u_j \rangle_L - \langle u_i \rangle_L \langle u_j \rangle_L],$$

$$(2.12) \quad \mathcal{Q}_i = -\langle \rho \rangle_l [\langle u_i E \rangle_L - \langle u_i \rangle_L \langle E \rangle_L].$$

Similarly, the filtered equation of state and the relation between filtered total energy and filtered sensible energy are:

$$(2.13) \quad \langle p \rangle_l = \langle \rho \rangle_l \langle RT \rangle_L,$$

$$(2.14) \quad \langle e \rangle_L = \langle E \rangle_L - \langle h_f^\circ \rangle_L - \frac{\langle u_i \rangle_L \langle u_i \rangle_L}{2} + \frac{\mathcal{S}_{ii}}{2 \langle \rho \rangle_l}.$$

The filtered mass flux, the filtered viscous term and the filtered heat flux and viscous dissipation are approximated as follows: [14,29](#)

$$(2.15) \quad \langle M_i^\alpha \rangle_l \simeq \langle \rho \rangle_l \langle \mathcal{D}_\alpha \rangle_l \frac{\partial \langle Y_\alpha \rangle_L}{\partial x_i},$$

$$(2.16) \quad \langle \sigma_{ij} \rangle_l \simeq \langle \mu \rangle_l \left(\frac{\partial \langle u_i \rangle_L}{\partial x_j} + \frac{\partial \langle u_j \rangle_L}{\partial x_i} - \frac{2}{3} \frac{\partial \langle u_k \rangle_L}{\partial x_k} \delta_{ij} \right),$$

$$(2.17) \quad \langle Q_i \rangle_l \simeq \left\langle \frac{\lambda}{C_p} \right\rangle_l \left(\frac{\partial \langle E \rangle_L}{\partial x_i} + \frac{\partial (\langle p \rangle_l / \langle \rho \rangle_l)}{\partial x_i} - \frac{1}{2} \frac{\partial (\langle u_j \rangle_l \langle u_j \rangle_l)}{\partial x_i} + \frac{1}{2} \frac{\partial (\mathcal{S}_{jj} / \langle \rho \rangle_l)}{\partial x_i} \right),$$

$$(2.18) \quad \langle \Phi \rangle_l \simeq \frac{\partial (\langle \sigma_{ij} \rangle_l \langle u_i \rangle_L)}{\partial x_j}.$$

The filtered material properties (\mathcal{D}_α , μ , λ and C_p) should also be approximated, if they are not constant.

The pressure-velocity gradient, $\partial\langle pu_i\rangle_i/\partial x_i$, can be transformed to the following alternative form:

$$\begin{aligned}
(2.19) \quad \frac{\partial\langle pu_i\rangle_i}{\partial x_i} &= \frac{\partial\langle\rho RTu_i\rangle_i}{\partial x_i} \\
&= \frac{\partial(\langle\rho\rangle_i\langle(\gamma-1)eu_i\rangle_L)}{\partial x_i} \\
&\simeq \frac{\partial(\langle\gamma-1\rangle_L\langle\rho\rangle_i\langle e\rangle_L\langle u_i\rangle_L)}{\partial x_i} - \frac{\partial(\langle\gamma-1\rangle_L\mathcal{Q}_i^{(s)})}{\partial x_i},
\end{aligned}$$

with the SGS sensible energy flux, $\mathcal{Q}_i^{(s)}$, given by (2.28). Finally, we assume,

$$\langle RT\rangle_L = \langle(\gamma-1)e\rangle_L \simeq \langle\gamma-1\rangle_L\langle e\rangle_L,$$

so that the equation of state can be written as

$$(2.20) \quad \langle p\rangle_i \simeq \langle\gamma-1\rangle_L\langle\rho\rangle_i\langle e\rangle_L.$$

In (2.19) and (2.20), the approximation is exact if γ is constant. Otherwise, we assume

$$\langle\gamma-1\rangle_L = \langle\gamma\rangle_L - 1 \simeq \frac{\langle C_p\rangle_L}{\langle C_v\rangle_L} - 1.$$

2.2 SUBGRID SCALE (SGS) CLOSURE

The SGS stress tensor is first decomposed into the isotropic, $\mathcal{S}_{ij}^{(I)}$, and the deviatoric, $\mathcal{S}_{ij}^{(D)}$, parts:

$$\mathcal{S}_{ij} = \mathcal{S}_{ij}^{(D)} + \mathcal{S}_{ij}^{(I)},$$

where

$$(2.21) \quad \mathcal{S}_{ij}^{(D)} = \mathcal{S}_{ij} - \frac{1}{3} \mathcal{S}_{kk} \delta_{ij}$$

and

$$(2.22) \quad \mathcal{S}_{ij}^{(I)} = \frac{1}{3} \mathcal{S}_{kk} \delta_{ij}.$$

The deviatoric part is modeled via the Smagorinsky model:^{14,34}

$$(2.23) \quad \mathcal{S}_{ij}^{(D)} = 2 \langle \rho \rangle_l \nu_T \left(\langle S_{ij} \rangle_L - \frac{1}{3} \langle S_{kk} \rangle_L \delta_{ij} \right),$$

where

$$(2.24) \quad \langle S_{ij} \rangle_L = \frac{1}{2} \left(\frac{\partial \langle u_i \rangle_L}{\partial x_j} + \frac{\partial \langle u_j \rangle_L}{\partial x_i} \right),$$

is the filtered rate of strain and ν_T is the SGS viscosity. The latter is modeled by

$$(2.25) \quad \nu_T = C_s l^2 \left(\langle S_{ij} \rangle_L \langle S_{ij} \rangle_L \right)^{\frac{1}{2}},$$

where $l = (\Delta_x \Delta_y \Delta_z)^{\frac{1}{3}}$ and Δ_x , Δ_y and Δ_z are the grid spacings in x -, y - and z -direction, respectively.³⁴ Here, x , y and z refer to stream-wise, cross-stream and span-wise directions. The parameter C_s is the Smagorinsky constant which is assigned a value or computed dynamically. For the isotropic part of SGS stress tensor, Yoshizawa model⁴¹ is used:

$$(2.26) \quad \mathcal{S}_{ij}^{(I)} = -\frac{2}{3} C_I \langle \rho \rangle_l l^2 \left(\langle S_{mn} \rangle_L \langle S_{mn} \rangle_L \right) \delta_{ij}.$$

with C_I being a constant.

The SGS total energy flux is split to three components:

$$(2.27) \quad \mathcal{Q}_i = \mathcal{Q}_i^{(s)} + \mathcal{Q}_i^{(c)} + \frac{1}{2} \mathcal{Q}_i^{(k)},$$

where

$$(2.28) \quad \mathcal{Q}_i^{(s)} = -\langle \rho \rangle_l [\langle u_i e \rangle_L - \langle u_i \rangle_L \langle e \rangle_L],$$

$$(2.29) \quad \mathcal{Q}_i^{(c)} = -\langle \rho \rangle_l [\langle u_i h_f^o \rangle_L - \langle u_i \rangle_L \langle h_f^o \rangle_L],$$

$$(2.30) \quad \mathcal{Q}_i^{(k)} = -\langle \rho \rangle_l [\langle u_i u_j u_j \rangle_L - \langle u_i \rangle_L \langle u_j u_j \rangle_L].$$

The term $\mathcal{Q}_i^{(s)}$ is the SGS heat flux and represents the subgrid transport of the sensible energy of the fluid, $\mathcal{Q}_i^{(c)}$ represents the SGS transport of chemical energy and $\mathcal{Q}_i^{(k)}$ is the SGS turbulent diffusion which measures the SGS kinetic energy transport.

Following Eidson,¹³ $\mathcal{Q}_i^{(s)}$ is modeled by

$$(2.31) \quad \mathcal{Q}_i^{(s)} = \frac{\langle \rho \rangle_l \nu_T}{Pr_T} \frac{\partial \langle e \rangle_L}{\partial x_i},$$

where Pr_T is the SGS Prandtl number (a model constant). For $\mathcal{Q}_i^{(c)}$, we note

$$(2.32) \quad \begin{aligned} \mathcal{Q}_i^{(c)} &= -\langle \rho \rangle_l [\langle u_i h_f^o \rangle_L - \langle u_i \rangle_L \langle h_f^o \rangle_L] \\ &= -\langle \rho \rangle_l [\langle u_i \sum_{\alpha=1}^N h_{f,\alpha}^o Y_\alpha \rangle_L - \langle u_i \rangle_L \langle \sum_{\alpha=1}^N h_{f,\alpha}^o Y_\alpha \rangle_L] \\ &= \sum_{\alpha=1}^N h_{f,\alpha}^o (-\langle \rho \rangle_l [\langle u_i Y_\alpha \rangle_L - \langle u_i \rangle_L \langle Y_\alpha \rangle_L]) \\ &= \sum_{\alpha=1}^N h_{f,\alpha}^o \mathcal{M}_i^\alpha \end{aligned}$$

where $h_{f,\alpha}^o$ is the mass enthalpy of formation of species α at 0K. In the second step we have used the fact that $h_{f,\alpha}^o$ is constant for each species. Equation (2.32) shows that there is no need to model $\mathcal{Q}_i^{(c)}$ separately. The model of Knight *et al.*²⁵ is used for closure of $\mathcal{Q}_i^{(k)}$:

$$(2.33) \quad \mathcal{Q}_i^{(k)} = u_j \mathcal{S}_{ij}.$$

Finally, \mathcal{M}_i^α , is modeled similar to SGS heat flux:²⁴

$$(2.34) \quad \mathcal{M}_i^\alpha = \frac{\langle \rho \rangle_l \nu_T}{Sc_T} \frac{\partial \langle Y_\alpha \rangle_L}{\partial x_i},$$

where Sc_T is the SGS Schmidt number (a model constant).

Three sets of simulations are conducted. These simulations differ in the way the model “constants” are implemented. Table 1 provides a listing of all these constants. These are either kept fixed or computed dynamically. In the latter, the dynamic procedure of Moin *et al.*²⁹ is used.

Table 1: Model constants.

Constant	Simulation I	Simulation II	Simulation III
C_s	0.014 (Erlebacher <i>et al.</i> ¹⁴)	Dynamic Model (Moin <i>et al.</i> ²⁹)	Dynamic Model (Moin <i>et al.</i> ²⁹)
C_I	0.0066 (Speziale <i>et al.</i> ³⁸)	0.0066 (Speziale <i>et al.</i> ³⁸)	0.0066 (Speziale <i>et al.</i> ³⁸)
Pr_T	0.75 (Eidson, ¹³ Cutler <i>et al.</i> ⁴)	Dynamic Model (Moin <i>et al.</i> ²⁹)	Dynamic Model (Moin <i>et al.</i> ²⁹)
Sc_T	equal to Pr_T (Cutler <i>et al.</i> ⁶)	equal to Pr_T (Cutler <i>et al.</i> ⁶)	Dynamic Model ^a (Moin <i>et al.</i> ²⁹)

^aMoin *et al.*²⁹ do not consider Sc_T . However, a similar method to that for Pr_T can be developed.

3.0 CONFIGURATION AND COMPUTATION

The flow configuration^{4,6} is shown in Figure 1 and consists of a non-reacting coaxial axisymmetric jet with a center jet composition of oxygen and helium (5% and 95% by volume, respectively) and a coflow of air. The diameters of the center jet and the coflow are 10mm and 60mm respectively. Measurements are provided from the nozzle exit to a downstream distance of 261mm. These include pressure, composition, total temperature and axial velocity.

Both streams are discharged to ambient at 1 atmosphere and at Mach 1.8. The velocity of the center jet, however, is more than that of the coflow since the jet is of a lighter gas with a higher speed of sound. The total temperature of both the center jet and the coflow is about 300K. A summary of important flow properties is given in Table 2. In this table N_x , N_y and N_z denote the number of grid points in x -, y - and z -directions, respectively. Also note that the origin of the Cartesian system is located on the centerline at the jet exit. The Reynolds and Mach numbers are defined by $Re = (U_{jet} D_{jet})/\nu_{jet}$ and $Ma = u/\sqrt{\gamma RT}$, respectively. Here, U_{jet} , D_{jet} and ν_{jet} are jet velocity, diameter and dynamic viscosity at the nozzle exit, respectively. The variables u , γ , R and T are velocity, specific heats ratio, gas constant and temperature of either the jet or the coflow mixture, respectively. Constants L_{ref} and U_{ref} are reference length and velocity (respectively), used in non-dimensionalization of equations.

Computations are performed with the two-four method of Gottlieb *et al.*²¹ on a domain of 121mm \times 50mm \times 50mm in x -, y - and z -directions with a Cartesian grid with 158 \times 65 \times 65 nodes, respectively.

The flowfield was initialized to the inlet averaged filtered values. At freestreams, zero derivative boundary condition is used⁹. At the outlet, in the case of supersonic outflow,

Table 2: Summary of flow and calculations parameters.^a

Total temperature: Center jet: 300 K Coflow: 300 K Diameters: Center jet: 10.00 mm Coflow: 60.47 mm	Total Pressure: Center jet: 522 kPa Coflow: 464 kPa Grid: $0 \leq x \leq 121$ $-25 \leq y, z \leq 25$ $N_x = 158$ $N_y = N_z = 65$
Non-dimensional and reference parameters	
$Re_D = 278000^b$, $Ma = 1.8^c$, $L_{ref} = 10$ mm, $U_{ref} = 487$ m/s	

^aApproximate values. See Cutler *et al.*^{4,6} for details.

^bBased on jet properties.

^cBased on either jet or coflow properties.

2nd order extrapolation is used; and at subsonic outflow, total pressure and temperature are specified and velocities and mass fractions are extrapolated.⁶ At the inflow, the average values from the experiment are specified for all variables, except for the inlet axial velocity, where small perturbations are superimposed on the mean profile at fundamental jet instability frequency and its first two sub-harmonics.²³

In dynamic simulations, the “test” filter was chosen to be twice the width of the primary filter (*i.e.*, two grid point averages in x -, y - and z -directions). The azimuthal (θ -direction) is considered homogeneous; thus averaging was performed on strips of $5 \times dy$ width. For stability, in dynamic simulations, the model constants were forced to be the same as the average value of the constants over the whole domain.

4.0 RESULTS

Figure 2 and 3 show the values of averaged filtered axial velocity, $\overline{\langle u \rangle_L}$, and averaged mass fraction of center jet, $\overline{\langle Y_{He-O_2} \rangle_L}$. Here, the over-bar denotes the ensemble average value. Results of Simulation II are very similar to those of Simulation III and hence are not shown. It is seen that, in general, the dynamic model provides better agreement for velocity, while $\overline{\langle Y_{He-O_2} \rangle_L}$ is predicted better in Simulation I. To investigate this issue, the values of C_s , Pr_T and Sc_T as obtained by dynamic models are given in Figures 4 and 5. It is readily seen that C_s values from Simulation III are, in average, higher than those in Simulation I. Also shown in Figure 4 is the value of C_s suggested by Rizzetta *et al.*³³. This is higher than both of the values incorporated here. Figure 5 indicates that the values of Pr_T and Sc_T are much higher in Simulations III compared to Simulation I. This is the primary reason for more accurate prediction of $\overline{\langle Y_{He-O_2} \rangle_L}$ via Simulation I. The fact that the variations of Sc_T , in this jet configuration, does not affect the results of the dynamic simulations significantly, can be attributed to the dominance of large scale mixing.

Plots of the resolved and residual components of the Reynolds Stress tensor and mass flux vector are shown in Figure 6 at selected stream-wise and span-wise locations. These quantities are defined by:

$$(4.1) \quad R(f_i, f_j) = \overline{\langle f_i \rangle_L \langle f_j \rangle_L} - \overline{\langle f_i \rangle_L} \overline{\langle f_j \rangle_L},$$

$$(4.2) \quad \overline{\tau^R(f_i, f_j)} = \overline{\langle f_i f_j \rangle_L} - \overline{\langle f_i \rangle_L} \overline{\langle f_j \rangle_L}.$$

As it is seen in Figure 6(a), the Smagorinsky model produces excessive dissipative nature (as expected). The overall ratio of resolved to residual Reynolds stress tensor (and mass flux vector) components are predicted better by Simulation III (and II).

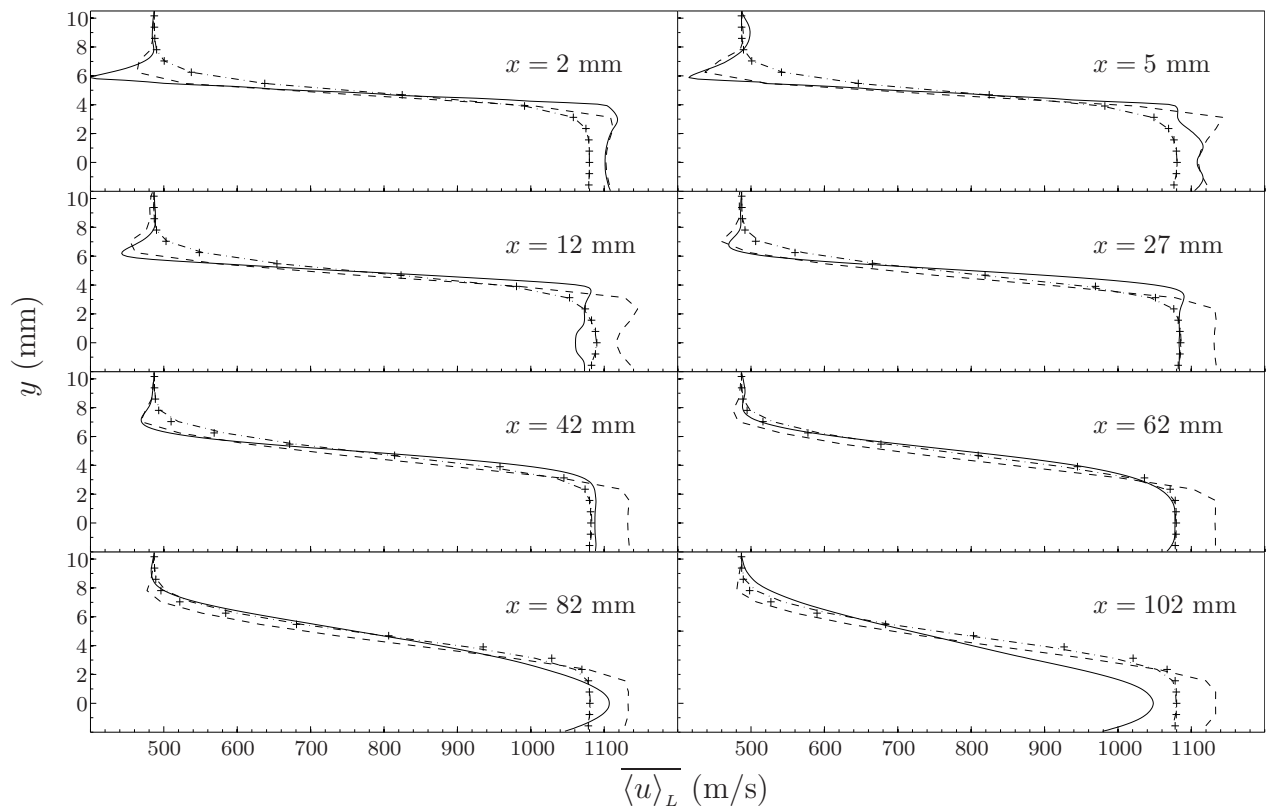


Figure 2: Average filtered velocity profiles. — Experiment, -- Simulation I, -.- Simulation III.

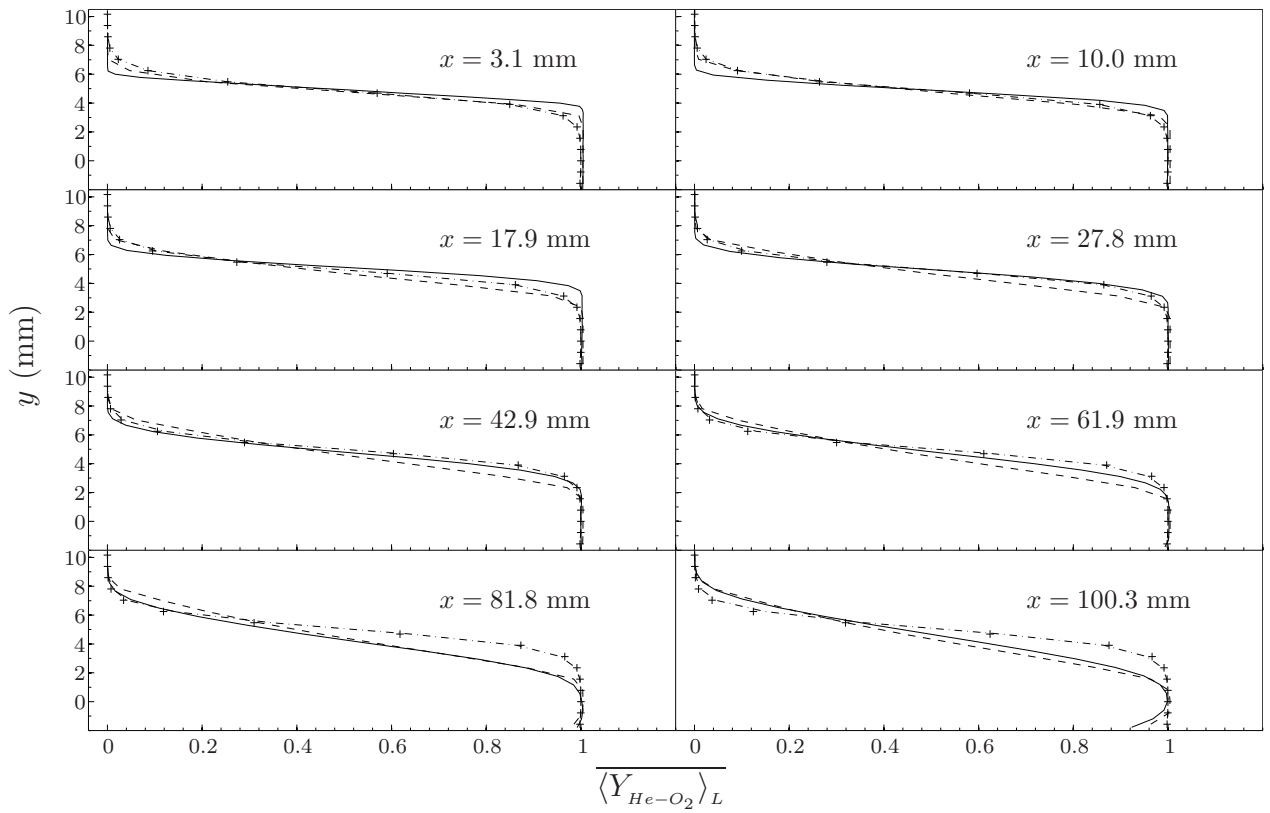


Figure 3: Profiles of average filtered mass fraction of center jet. — Experiment, -- Simulation I, -.- Simulation III.

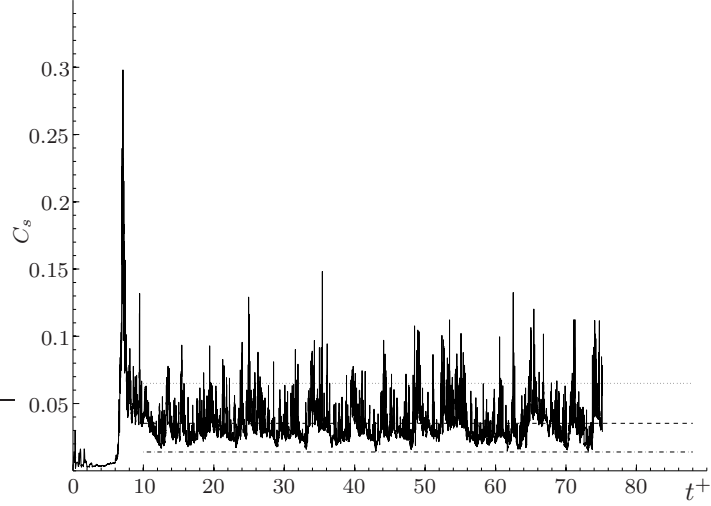


Figure 4: Computed values of Smagorinsky coefficient versus time. — time history from Simulation III, -- average value from Simulation III, -.- average value from Simulation I, ... value used by Rizzetta *et al.*³³ ($t^+ = (tU_{ref})/L_{ref}$)

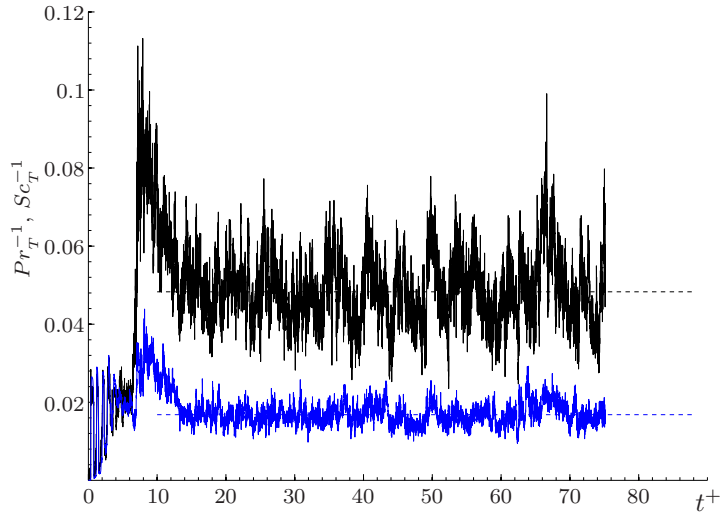


Figure 5: Computed SGS Prandtl and Schmidt numbers from dynamic Simulations: Pr_T^{-1} (black) and Sc_T^{-1} (blue) time histories. ($t^+ = (tU_{ref})/L_{ref}$)

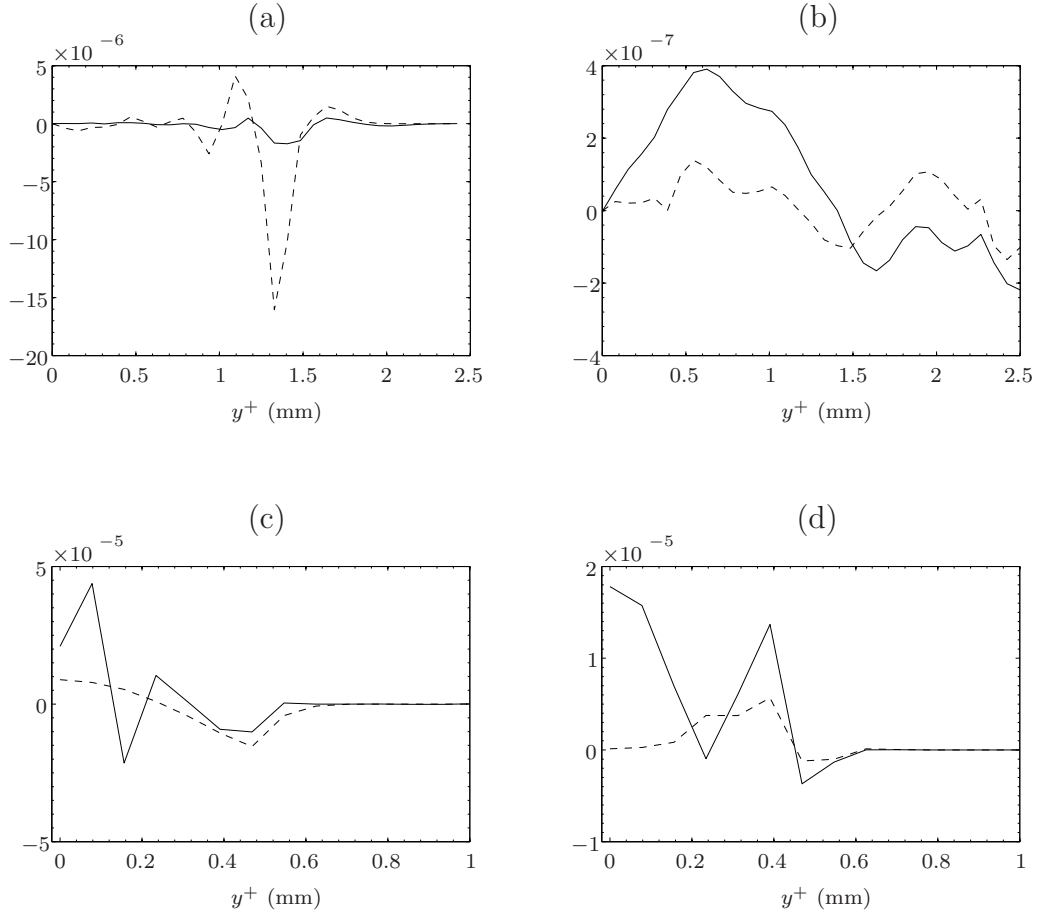


Figure 6: Resolved and residual portions of turbulent stresses and fluxes. (a) Simulation I: $-R(u, v)$, $-- \overline{\tau^R(u, v)}$. (b) Simulation III: $-R(u, v)$, $-- \overline{\tau^R(u, v)}$. (c) Simulation I: $-R(u, Y_{He-O_2})$, $-- \overline{\tau^R(u, Y_{He-O_2})}$. (d) Simulation III: $-R(u, Y_{He-O_2})$, $-- \overline{\tau^R(u, Y_{He-O_2})}$. ($y^+ = y/L_{ref}$)

The instantaneous contour plot of filtered pressure at $t^+ = 71.67$ ($t^+ = (tU_{ref})/L_{ref}$), is shown in Figure 7. As expected, Variations of pressure are small as predicted by Cutler *et al.*^{4,6} Evaluation of the filtered Mach number, Ma , is not possible since it is a nonlinear function of the principal flow variables; However, the following approximation can be used to facilitate a qualitative investigation of Mach number variations throughout the domain:

$$\langle Ma \rangle_L = \left(\frac{\langle \rho \rangle_l \langle u_k \rangle_L \langle u_k \rangle_L + \mathcal{S}_{kk}}{\langle \gamma \rangle_l \langle p \rangle_l} \right)^{\frac{1}{2}}.$$

Figure 8 shows the contour plots of the average Mach number and indicates that subsonic flow regions are not likely to exist in the flow domain considered in the simulations. As noted previously the mixing layers at the nozzle outlet are compressible. These compressibility effects can be seen in Figure 9 which shows the instantaneous density contour plot at $t^+ = 299.13$ ($t^+ = tU_{ref}/L_{ref}$). As the flow propagates in the domain these effects diminish, which is consistent with laboratory experiments where no strong shock waves were observed in downstream regions.

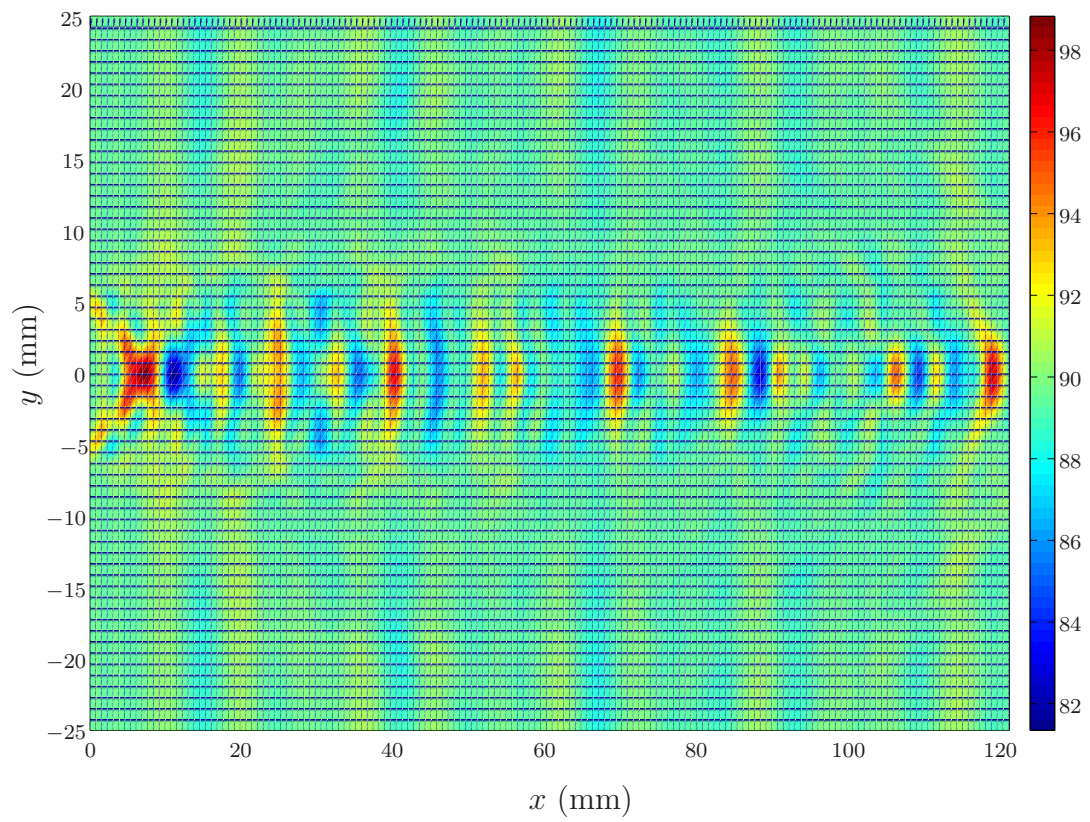


Figure 7: Contour plot of the instantaneous values of $\langle p \rangle_i$ (kPa) at $t^+ = 71.67$ (Simulation III).

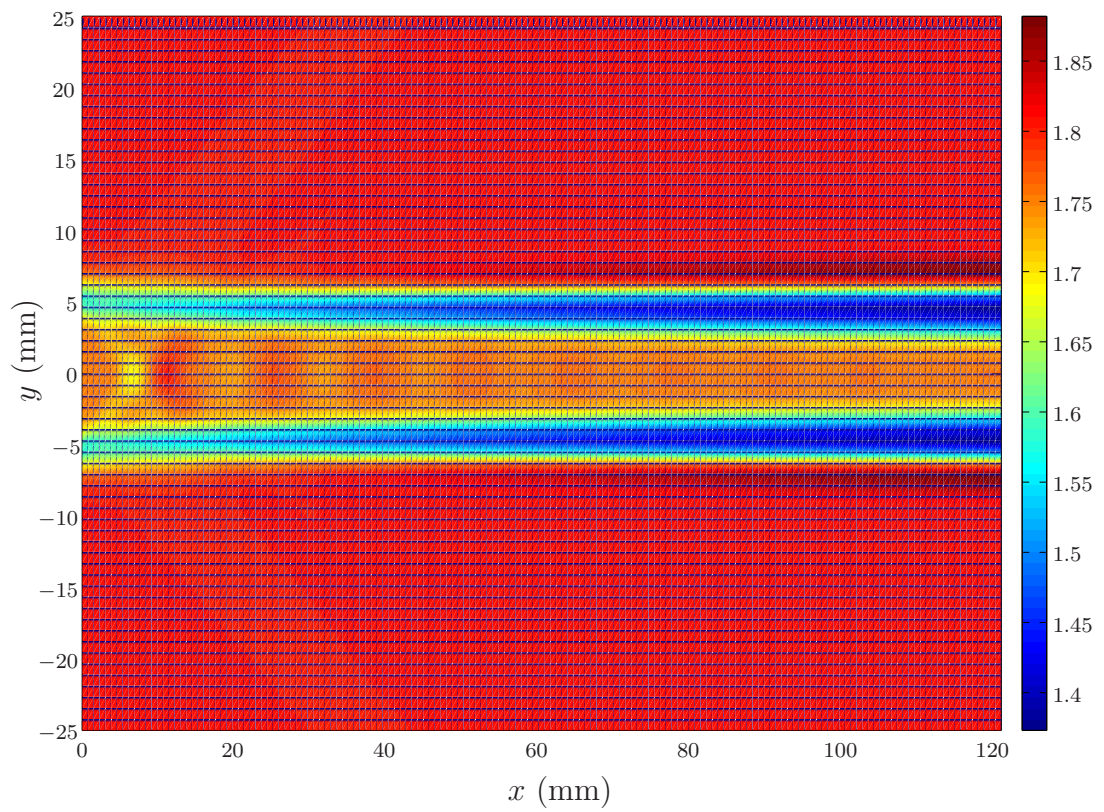


Figure 8: Contour plot of the Reynolds averaged values of the Mach number (Simulation III).

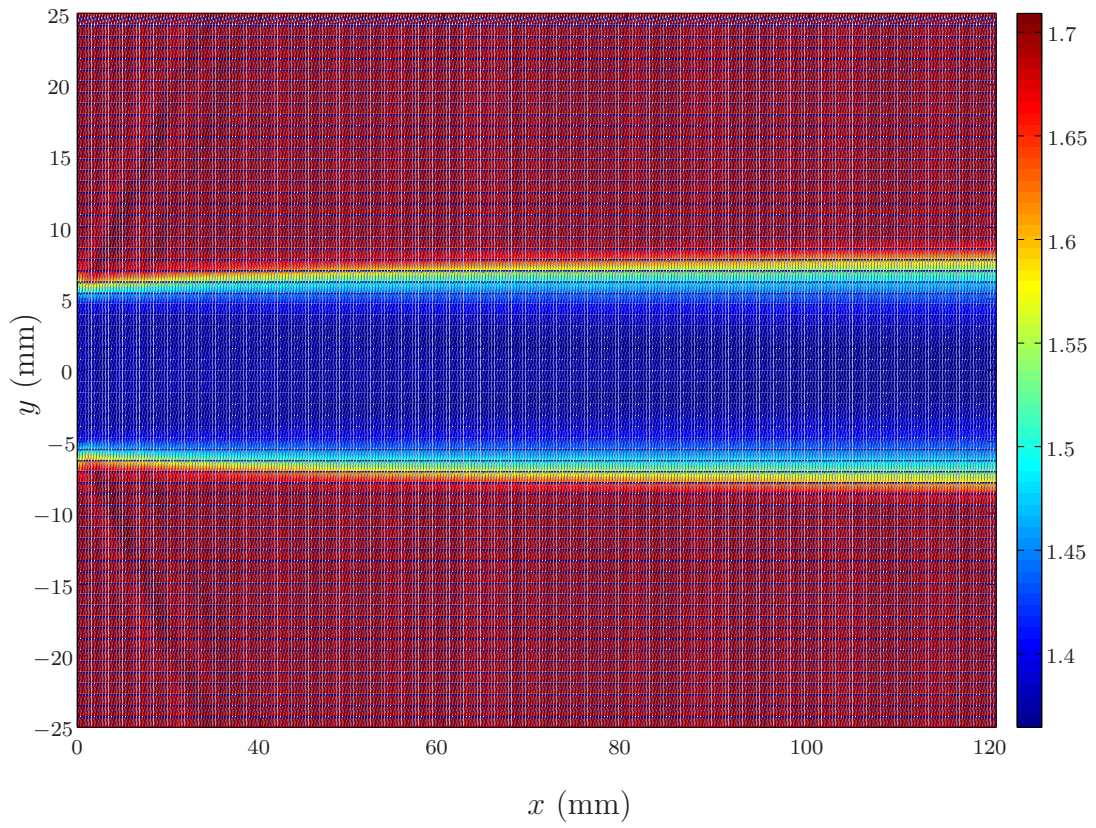


Figure 9: Contour plot of the instantaneous values of the filtered density (kg/m³) at $t^+ = 299.13$ (Simulation I).

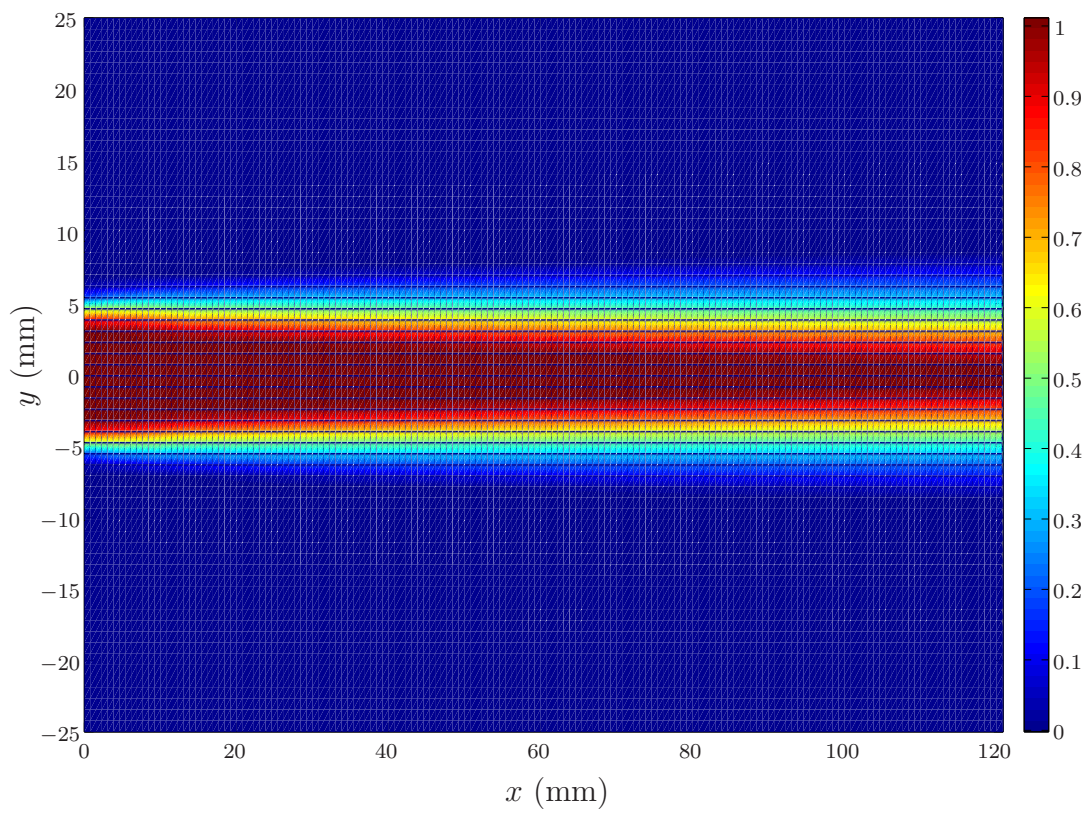


Figure 10: Contour plot of the Reynolds averaged values of $\langle Y_{He-O_2} \rangle_L$ from Simulation I.

5.0 CONCLUSIONS

Large-eddy simulation of a supersonic coaxial jet is conducted using the Smagorinsky and the dynamic models. The configuration consists of a coaxial jet discharging into stagnant air with the main stream of He-O₂ (95% Helium and 5% Oxygen by volume, respectively) and a coflow of air. The filtered compressible, 3-dimensional Navier-Stokes equations for a mutli-species system are solved and the predicted results are assessed via comparison with experimental data from the Hypersonic Air-breathing Propulsion Branch at the NASA Langly Research Center. The objective of this work is to investigate the performance of the hydrodynamic closures in high speed flows.

The dynamic model provides better overall results for filtered velocity. Simulations with this model yield higher values for the Smagorinsky coefficient, C_s , than the values suggested for incompressible flows. On the other hand, the filtered mass fraction of the center jet is predicted more accurately via the Smagorinsky model. Here, again the dynamic model gives higher values for model coefficients Pr_T and Sc_T . While computed values of these two parameters are not equal (suggesting that the SGS heat and mass diffusions are not comparable), the results of the dynamic model are found to be insensitive to variations of Sc_T when this parameter is computed dynamically (Simulation III) or is assigned a value (Simulation II).

The predicted results are, generally, in good agreement with laboratory data as far as first moments are concerned. The simulations suggest that the dynamic model provides a better allocation of resolved and residual stresses.

BIBLIOGRAPHY

- [1] R. W. Bilger. Future progress in turbulent combustion research. *Progress in Energy and Combustion Science*, 26(4–6):367–380, 2000.
- [2] P. J. Colucci, F. A. Jaber, P. Givi, and S. B. Pope. Filtered density function for large-eddy simulation of turbulent reacting flows. *Physics of Fluids*, 10(2):499–515, 1998.
- [3] A. D. Cutler, P. M. Danehy, R. R. Springer, S. O’Byrne, and D. P. Capriotti. Coherent anti-Stokes Raman spectroscopic thermometry in a supersonic combustor. *AIAA Journal*, 41(12):2451–2459, 2003.
- [4] A. D. Cutler, G. S. Diskin, P. M. Danehy, and J. P. Drummond. Fundamental mixing and combustion experiments for propelled hypersonic flight. AIAA Paper 2002-3879, AIAA, Washington, D.C., 2002.
- [5] A. D. Cutler, G. S. Diskin, J. P. Drummond, and J. A. White. Supersonic coaxial jet experiment for computational fluid dynamics code validation. *AIAA Journal*, 44(3):585–592, 2006.
- [6] A. D. Cutler and J. A. White. An experimental and CFD study of a supersonic coaxial jet. AIAA Paper 2001-0143, AIAA, Washington, D.C., 2001.
- [7] T. G. Drozda. *Large-eddy Simulation of a Piloted Diffusion Flame (Sandia Flame D) and a Bluff-Body Flame (Sydney Flame)*. PhD Thesis, University of Pittsburgh, Pittsburgh, PA, 2005.
- [8] T. G. Drozda, M. R. H. Sheikhi, C. K. Madnia, and P. Givi. Developments in formulation and application of the filtered density function. *Flow, Turbulence and Combustion*, 78(1):35–67, 2007.
- [9] J. P. Drummond. A two-dimensional numerical simulation of a supersonic, chemically reacting mixing layer. Technical Report NASA TM-4055, NASA Langley Research Center, Hampton, VA, 1988.
- [10] J. P. Drummond. Supersonic reacting internal flow fields. In E. S. Oran and J. P. Boris, editors, *Numerical Approaches to Combustion Modeling, Progress in Astronautics and*

- Aeronautics*, volume 135, chapter 12, pages 365–420. AIAA Publishing Co., Washington, D.C., 1991.
- [11] J. P. Drummond, M. H. Carpenter, and D. W. Riggins. Mixing and mixing enhancements in supersonic reacting flow fields. In S. N. B. Murthy and E. T. Curran, editors, *High Speed Propulsion Systems, AIAA Progress Series*, volume 137, chapter 7, pages 383–455. AIAA, Washington, D.C., 1991.
- [12] J. P. Drummond, P. M. Danehy, D. Bivolaru, R. L. Gaffney, P. A. Parker, H. K. Chelliah, A. D. Cutler, P. Givi, and H. A. Hassan. Predicting the effects of test media in ground-based propulsion testing. *Annual ITEA Technology Review*, Cambridge, MA, August 7–10 2006.
- [13] T. M. Eidson. Numerical simulation of the turbulent Rayleigh-Bénard problem using subgrid modelling. *Journal of Fluid Mechanics*, 158:245–268, 1985.
- [14] G. Erlebacher, M. Y. Hussaini, C. G. Speziale, and T. A. Zang. Toward the large-eddy simulation of compressible turbulent flows. *Journal of Fluid Mechanics*, 238:155–185, 1992.
- [15] S. H. Frankel, V. Adumitroaie, C. K. Madnia, and P. Givi. Large-eddy simulations of turbulent reacting flows by assumed PDF methods. In S. A. Ragab and U. Piomelli, editors, *Engineering Applications of Large-eddy Simulations*, pages 81–101. ASME FED-Vol. 162, New York, NY, 1993.
- [16] S. C. Garrick, F. A. Jaber, and P. Givi. Large-eddy simulation of scalar transport in a turbulent jet flow. In D. Knight and L. Sakell, editors, *Recent Advances in DNS and LES, Fluid Mechanics and its Applications*, pages 155–166. Kluwer Academic Publishers, The Netherlands, vol. 54 edition, 1999.
- [17] L. Y. M. Gicquel, P. Givi, F. A. Jaber, and S. B. Pope. Velocity filtered density function for large-eddy simulation of a turbulent mixing layer. In C. Liu, L. Sakell, and R. Herklotz, editors, *DNS/LES-Progress and Challenges*, pages 327–334. Greyden Press, Columbus, OH, 2001.
- [18] L. Y. M. Gicquel, P. Givi, F. A. Jaber, and S. B. Pope. Velocity filtered density function for large-eddy simulation of turbulent flows. *Physics of Fluids*, 14(3):1196–1213, 2002.
- [19] P. Givi. Model free simulations of turbulent reactive flows. *Progress in Energy and Combustion Science*, 15(1):1–107, 1989.
- [20] P. Givi. Filtered density function for subgrid scale modeling of turbulent combustion. *AIAA Journal*, 44(1):16–23, 2006.
- [21] D. Gottlieb and E. Turkel. Dissipative tow-four methods for time-dependent problems. *Mathematics of Computation*, 30(136):703–723, 1976.
- [22] J. O. Hinze. *Turbulence*. McGraw-Hill, New York, 1975.

- [23] C. M. Ho and P. Huerrer. Perturbed free shear layers. *Annual Reviews of Fluids Mechanics*, 19:365–42, 1984.
- [24] F. A. Jaber, P. J. Colucci, S. James, P. Givi, and S. B. Pope. Filtered mass density function for large-eddy simulation of turbulent reacting flows. *Journal of Fluid Mechanics*, 401:85–121, 1999.
- [25] D. Knight, G. Zhou, N. Okong’o, and V. Shukla. Compressible large-eddy simulation using unstructured grids. AIAA Paper 98-0535, AIAA, Washington, D.C., 1998.
- [26] A. Leonard. Energy cascade in large-eddy simulations of turbulent fluid flows. *Advances in Geophysics*, 18:273–248, 1974.
- [27] P. A. Libby and F. A. Williams, editors. *Turbulent Reacting Flows*. Academic Press, London, 1994.
- [28] C. K. Madnia and P. Givi. Direct numerical simulation and large-eddy simulation of reacting homogeneous turbulence. In B. Galperin and S. A. Orszag, editors, *Large-eddy Simulations of Complex Engineering and Geophysical Flows*, pages 315–346. Cambridge University Press, Cambridge, England, 1993.
- [29] P. Moin, K. D. Squires, W. Cabot, and S. Lee. A dynamic subgrid scale model for compressible turbulence and scalar transport. *Physics of Fluids A*, 3(11):2746–2757, 1991.
- [30] T. Poinso and D. Veynante. *Theoretical and Numerical Combustion*. R.T. Edwards Inc., Philadelphia, second edition, 2001.
- [31] S. B. Pope. Computations of turbulent combustion: Progress and challenges. *Proceedings of the Combustion Institute*, 23:591–612, 1990.
- [32] S. B. Pope. *Turbulent Flows*. Cambridge University Press, Cambridge, 2000.
- [33] D. P. Rizzetta and M. R. Visbal. Large-eddy simulation of supersonic boundary-layer flow by a high-order method. *International Journal of Computational Fluid Dynamics*, 18(1):15–27, 2004.
- [34] A. Scotti, C. Meneveau, and D. K. Lilly. Generalized Smagorinsky model for anisotropic grids. *Physics of Fluids A*, 5(9):2306–2308, 1993.
- [35] M. R. H. Sheikhi. *Joint Velocity-Scalar Filtered Density Function for Large-eddy Simulation of Turbulent Reacting Flows*. PhD Thesis, University of Pittsburgh, Pittsburgh, PA, 2005.
- [36] M. R. H. Sheikhi, T. G. Drozda, P. Givi, and S. B. Pope. Velocity-scalar filtered density function for large-eddy simulation of turbulent flows. *Physics of Fluids*, 15(8):2321–2337, 2003.

- [37] M. R. H. Sheikhi, P. Givi, and S. B. Pope. Large-eddy simulation of a turbulent non-premixed piloted methane jet flame (Sandia flame D). In *Proceedings of the Combustion Institute*, volume 30, pages 549–55, 2005.
- [38] C. G. Speziale, G. Erlebacher, T. A. Zang, and M. Y. Hussaini. The subgrid scale modeling of compressible turbulence. *Physics of Fluids*, 31(4):940–942, 1988.
- [39] M. E. White, J. P. Drummond, and A. Kumar. Evolution and application of CFD techniques for scramjet engine applications. *Journal of Propulsion and Power*, 3(5):423–439, 1987.
- [40] F. A. Williams. *Combustion Theory: The Fundamental Theory of Chemically Reacting Flow Systems*. Benjamin Cummings Pub. Co., second edition, Menlo Park, CA, 1985.
- [41] A. Yoshizawa. Statistical theory of compressible turbulent shear flows, with the application to subgrid modeling. *Physics of Fluids*, 29(7):2152–2164, 1986.